Research Article | Vol. 7, No. 11 | 1 Nov 2016 | BIOMEDICAL OPTICS EXPRESS 4685

Biomedical Optics EXPRESS

In-vivo monitoring of tissue oxygen saturation in deep brain structures using a single fiber optical system

LINHUI YU,[1] YING WU,[2] JEFF F. DUNN,[2,3,4] AND KARTIKEYA MURARI[1,3,*]

[1]*Electrical and Computer Engineering, Schulich School of Engineering, University of Calgary, Canada*
[2]*Department of Radiology, Cumming School of Medicine, University of Calgary, Canada*
[3]*Hotchkiss Brain Institute, University of Calgary, Canada*
[4]*Experimental Imaging Centre, University of Calgary, Canada*
[*]*kmurari@ucalgary.ca*

Abstract: We propose a single fiber optical system for monitoring tissue oxygen saturation (sO_2) based on continuous-wave reflectance spectroscopy in the visible wavelengths. The system is designed for measurements in deep brain structures by stereotaxically implanting the 200 μm-core fiber probe into the tissue of interest. Monte Carlo (MC) simulations were used to estimate the measurement tissue volume between 0.02-0.03 mm^3. Experiments in an optical phantom indicated the system had a root mean squared error (RMSE) of 4.21% compared with a commercial fluorescence-based tissue oxygen partial pressure measuring system. Finally, we used the system for continuously monitoring tissue sO_2 from a highly-localized volume in anesthetized mice.

OCIS codes: (170.3890) Medical optics instrumentation; (170.6510) Spectroscopy, tissue diagnostics; (170.1470) Blood or tissue constituent monitoring; (170.3660) Light propagation in tissues.

References and links

1. E. M. Hillman, "Optical brain imaging in vivo: techniques and applications from animal to man," J. Biomed. Opt. **12**, 051402 (2007).
2. T. Vo-Dinh, *Biomedical Photonics Handbook: Biomedical Diagnostics* (CRC Press, 2014).
3. M. Ferrari and V. Quaresima, "A brief review on the history of human functional near-infrared spectroscopy (fNIRS) development and fields of application," Neuroimage **63**, 921–935 (2012).
4. E. E. Hoover and J. A. Squier, "Advances in multiphoton microscopy technology," Nat. Photonics **7**, 93–101 (2013).
5. F. Zhang, V. Gradinaru, A. R. Adamantidis, R. Durand, R. D. Airan, L. de Lecea, and K. Deisseroth, "Optogenetic interrogation of neural circuits: technology for probing mammalian brain structures," Nat. Protoc. **5**, 439–456 (2010).
6. J. Griffiths and S. Robinson, "The OxyLite: A fibre-optic oxygen sensor," Brit. J. Radiol. **72**, 627–630 (1999).
7. E. Ortiz-Prado, S. Natah, S. Srinivasan, and J. F. Dunn, "A method for measuring brain partial pressure of oxygen in unanesthetized unrestrained subjects: The effect of acute and chronic hypoxia on brain tissue pO_2," J. Neurosci. Methods **193**, 217–225 (2010).
8. H. Adelsberger, O. Garaschuk, and A. Konnerth, "Cortical calcium waves in resting newborn mice," Nat. Neurosci. **8**, 988–990 (2005).
9. K. Schulz, E. Sydekum, R. Krueppel, C. J. Engelbrecht, F. Schlegel, A. Schröter, M. Rudin, and F. Helmchen, "Simultaneous bold fMRI and fiber-optic calcium recording in rat neocortex," Nat. Methods **9**, 597–602 (2012).
10. A. Stroh, H. Adelsberger, A. Groh, C. Rühlmann, S. Fischer, A. Schierloh, K. Deisseroth, and A. Konnerth, "Making waves: initiation and propagation of corticothalamic Ca^{2+} waves in vivo," Neuron **77**, 1136–1150 (2013).
11. R. Pashaie and R. Falk, "Single optical fiber probe for fluorescence detection and optogenetic stimulation," IEEE Trans. Biomed. Eng. **60**, 268–280 (2013).
12. L. A. Gunaydin, L. Grosenick, J. C. Finkelstein, I. V. Kauvar, L. E. Fenno, A. Adhikari, S. Lammel, J. J. Mirzabekov, R. D. Airan, K. A. Zalocusky, K. M. Tye, P. Anikeeva, R. C. Malenka, and K. Deisseroth, "Natural neural projection dynamics underlying social behavior," Cell **157**, 1535–1551 (2014).
13. L. Yu, K. Ronayne, T. Johnson, T. Fuzesi, J. Dunn, J. Bains, and K. Murari, "Single fiber optical systems for monitoring brain dynamics in deep structures," in "Bio-Optics: Design and Application," (Optical Society of America, 2015), pp. JT3A–49.
14. S. C. Kanick, C. Van der Leest, J. G. Aerts, H. C. Hoogsteden, S. Kaščáková, H. J. Sterenborg, and A. Amelink, "Integration of single-fiber reflectance spectroscopy into ultrasound-guided endoscopic lung cancer staging of mediastinal lymph nodes," J. Biomed. Opt. **15**, 017004 (2010).

#273731 http://dx.doi.org/10.1364/BOE.7.004685
Journal © 2016 Received 17 Aug 2016; revised 5 Oct 2016; accepted 13 Oct 2016; published 21 Oct 2016

Biomedical Optics EXPRESS

15. S. H. Tabrizi, S. M. R. Aghamiri, F. Farzaneh, A. Amelink, and H. J. Sterenborg, "Single fiber reflectance spectroscopy on cervical premalignancies: the potential for reduction of the number of unnecessary biopsies," J. Biomed. Opt. **18**, 017002 (2013).
16. A. Sircan-Kuçuksayan, T. Denkceken, and M. Canpolat, "Differentiating cancerous tissues from noncancerous tissues using single-fiber reflectance spectroscopy with different fiber diameters," J. Biomed. Opt. **20**, 115007 (2015).
17. L. Yu and K. Murari, "Design of a single-fiber, wavelength-resolved system for monitoring deep tissue oxygenation," Proceedings of the 36th Annual Conference of the IEEE Engineering in Medicine and Biology Society pp. 3707–3710 (2014).
18. *Physical properties of glycerine and its solutions* (Glycerine Producers' Association, 1963).
19. S. Kanick, H. Sterenborg, and A. Amelink, "Empirical model of the photon path length for a single fiber reflectance spectroscopy device," Opt. Express **17**, 860–871 (2009).
20. S. C. Kanick, C. van der Leest, R. S. Djamin, A. M. Janssens, H. C. Hoogsteden, H. J. Sterenborg, A. Amelink, and J. G. Aerts, "Characterization of mediastinal lymph node physiology in vivo by optical spectroscopy during endoscopic ultrasound-guided fine needle aspiration," J. Thorac. Oncol. **5**, 981–987 (2010).
21. L. Wang, S. L. Jacques, and L. Zheng, "MCML: Monte Carlo modeling of light transport in multi-layered tissues," Comput. Methods Programs Biomed. **47**, 131–146 (1995).
22. J. F. Dunn, Q. Zhang, Y. Wu, S. Srinivasan, M. R. Smith, and R. A. Shaw, "Monitoring angiogenesis noninvasively with near-infrared spectroscopy," J. Biomed. Opt. **13**, 064043 (2008).
23. H. J. Van Staveren, C. J. Moes, J. van Marie, S. A. Prahl, and M. J. Van Gemert, "Light scattering in lntralipid-10% in the wavelength range of 400–1100 nm," Appl. Opt. **30**, 4507–4514 (1991).
24. H. Liu, Y. Gu, J. G. Kim, and R. P. Mason, "Near-infrared spectroscopy and imaging of tumor vascular oxygenation," Methods Enzymol. **386**, 349–378 (2004).
25. C.-F. Cartheuser, "Standard and pH-affected hemoglobin-O_2 binding curves of sprague-dawley rats under normal and shifted P50 conditions," Comp. Biochem. Physiol. Comp. Physiol. **106**, 775–782 (1993).
26. A. Amelink, T. Christiaanse, and H. J. Sterenborg, "Effect of hemoglobin extinction spectra on optical spectroscopic measurements of blood oxygen saturation," Opt. Lett. **34**, 1525–1527 (2009).
27. W. G. Zijlstra, A. Buursma, and O. W. van Assendelft, *Visible and Near Infrared Absorption Spectra of Human and Animal Haemoglobin: Determination and Application* (VSP, 2000).
28. B. Weber and F. Helmchen, *Optical Imaging of Neocortical Dynamics* (Springer, 2014).

1. Introduction

Functional monitoring of brain activity in deep brain structures is of great interest for both behavioral and pathological studies, however, optical methods for interrogating brain activity have limited depth of penetration because of tissue scattering. Traditionally, non-optical methods, functional magnetic resonance imaging (fMRI) and positron emission tomography (PET) for example, are used for monitoring activity in deep brain structures non-invasively [1]. Such methods are costly and usually require the animal to be restricted or anesthetized, which greatly limit the scope of studies. Near infrared wavelengths can reduce the effect of light scattering, thereby provide near infrared spectroscopy (NIRS) and two-photon excitation with the ability to reach deeper brain structures [2]. However, NIRS has limited spatial resolution [3], while two-photon imaging provides high spatial resolution with depth penetration limited to under 1 mm [4].

Another approach to interrogate the brain activity in deep structures is to use a single fiber probe to deliver and collect light from a highly-localized volume of tissue near the fiber tip. The fiber can be stereotactically inserted into the region of interest at any depth. Though invasive, it has been reported that implantation of a single fiber probe with a diameter less than 300 μm is safe for use in mice [5]. Thus, single fiber systems are ideal for the measurements of brain activity from a highly-localized volume in unconstrained animals in a cost-effective manner. So far, for functional monitoring of brain activity, single fiber systems have been used for measuring partial pressure of oxygen in freely-moving animals based on fluorescence quenching [6, 7] and fluorescence detection of calcium signals [8–13]. For other applications, single fiber systems have previously been reported for assisting lymph node biopsy [14] and cervical intraepithelial neoplasia detection [15] by estimating vascular oxygen saturation and blood volume fraction, and identifying cancerous tissues based on the spectral slopes [16].

We propose a single fiber system for monitoring sO_2 in deep brain structures using continuous-

Biomedical Optics EXPRESS

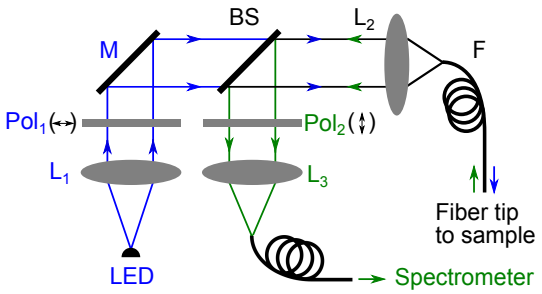

Fig. 1. Schematic drawing of the system showing light emitting diode (LED), collimating lens (L_1), mirror (M), beam splitter (BS), focusing lenses (L_2, L_3), fiber (F), polarizers (Pol_1, Pol_2) and spectrometer (S).

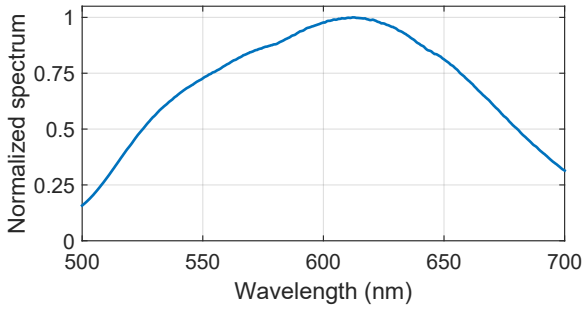

Fig. 2. Normalized spectrum in 500-700 nm of the warm white LED.

wave reflectance spectroscopy using 500-700 nm light. In this region, hemoglobin absorption is strong, thus it reduces the volume from which light is collected. This paper presents the optical design and simulations, measurement technique and experimental data in an optical phantom and *in-vivo*. To our knowledge, this is the first system capable of continuously monitoring sO_2 *in-vivo* at any depth in the brain from a highly-localized volume, albeit with the minimally invasive stereotaxic implantation of an optical fiber into the brain region of interest.

2. Material and methods

2.1. Optical system design

We have previously presented the design of the single fiber system and shown proof-of-concept data for measuring sO_2 [17]. Distinct from previously reported single fiber systems for reflectance spectroscopy [14, 16], our system avoids using high power light sources and delicate bifurcated fibers, giving it the potential for future miniaturization to a stand-alone head-mounted device for freely-moving animals.

Figure 1 shows a schematic drawing of the system. The delivery path (marked in blue) delivers the light from a warm white LED (334-15/X1C1-1TWA, Everlight Electronics Co Ltd, Taiwan) into the sample, and the collection path (marked in green) collects the light from the sample back to the spectrometer. In the delivery path, the light is collimated by a lens (L_1), and linearly polarized with a polarizer (Pol_1). 50% of the light is lost at the 50:50 beam splitter (BS). Then, the light is focused into a 200-μm-core, 0.39 NA fiber (F) by a second lens (L_2). Finally, the fiber delivers the light into the sample. In the collection path, the fiber collects light from the sample. The light coming out of the fiber is collimated by L_2. Then, half of this light is reflected 90° and

Biomedical Optics EXPRESS

goes through a second polarizer Pol_2, crossed to Pol_1. The light is focused into the spectrometer by a focusing lens (L_3). Figure 2 shows the normalized spectrum of the warm white LED in 500-700 nm.

2.2. Calibration

To account for the Fresnel reflections from the fiber end surfaces and the internal spectral attenuation caused by the optical components, we proposed a novel calibration method to calculate reflectance spectrum. The reflectance spectrum is defined as:

$$R = \frac{I_{sig}}{I_{in}} \tag{1}$$

where I_{in} and I_{sig} are the spectra of the incident light that enters and the signal-carrying light that exits the sample, respectively.

Using the proposed single fiber system, I_{sig} cannot be measured directly. When the fiber tip is in the sample, the spectrometer collects the signal light as well as Fresnel reflected light, which has not interacted with the sample, from the air-fiber and fiber-sample interfaces. These reflections are unrelated to the signal and have to be minimized to avoid saturating the detector. Pol_1 and Pol_2 cancel the reflection from the air-fiber interface at the near end of the fiber. The reflection from the fiber-sample interface is not removed in the system. It is estimated as the spectrum collected by the system when the fiber is in a sample matching medium (S_{mat}) and removed in the analysis. Moreover, the signal light exiting the sample is collected by the fiber and goes through the collection path. It experiences a wavelength-dependent attenuation introduced by the optical components in the system.

To correct these, we use the reflection from the fiber-sample interface to approximate the spectrum of the input light (I_{in}) with the attenuation in the collection path. It can be measured as the difference between the spectra collected when the fiber tip is in air (S_{air}) and when in glycerin (S_{gly}). When the fiber tip is in the air, S_{air} collects the Fresnel reflections from the fiber tip and also from the near end of the fiber that has not been removed by the polarizers. When the fiber tip is in glycerin, whose refractive index of 1.47 is very close to the 1.46 refractive index of the fiber, we assume that there is no reflection at the fiber tip. Thus, S_{gly} measures the residual reflection from the fiber near end. Therefore, (S_{air}-S_{gly}) measures the spectrum of I_{in} with the attenuation in the collection path. Then, the spectrum of I_{sig} with the same attenuation can be estimated using the difference between the spectra collected when the fiber tip is in the sample (S_{sam}) and in the matching medium which matches the sample refractive index (S_{mat}). In the phantom experiment, phosphate-buffered saline (PBS) was used as the matching medium. For the *in-vivo* experiment, a 22% glycerin-water solution, with the refractive index of 1.36, which matches that of brain tissue was used [2, 18]. Thus, the reflectance spectrum for our single fiber system, R_{SF} can be calculated as:

$$R_{SF} = \frac{S_{sam} - S_{mat}}{S_{air} - S_{gly}} \tag{2}$$

The wavelength-dependent attenuation cancels in the division.

2.3. Empirical model for single fiber reflectance spectroscopy

To extract sO_2 from the corrected spectrum R_{SF}, Kanick's empirical model [19] for single fiber reflectance spectroscopy is adapted in this research:

$$R_{SF} = R_0 e^{-\mu_a L_{SF}} \tag{3}$$

where R_0 is the reflectance spectrum with no absorbers, μ_a is the absorption coefficient, and L_{SF} is the single fiber path length. Assuming that the only chromophores in the brain are

Biomedical Optics EXPRESS

oxy-hemoglobin (HbO) and deoxy-hemoglobin (Hb), μ_a can be expressed as

$$\mu_a = C_v \rho \left(sO_2 \cdot \mu_{aHbO} + (1 - sO_2) \cdot \mu_{aHb}\right) \tag{4}$$

where C_v accounts for the pigment packaging effect, ρ is the total concentration of hemoglobin, and μ_{aHbO} and μ_{aHb} are the molar absorption coefficients of HbO and Hb. The empirical equation of the path length is:

$$L_{SF} = \frac{1.54 d_{fiber}}{(\mu_s' d_{fiber})^{0.18} \left(0.61 + (\mu_a d_{fiber})^{0.61}\right)} \tag{5}$$

where μ_s' is the reduced scattering coefficient, d_{fiber} is the diameter of the fiber. Eq. (6) models μ_s' using Mie scattering approximation [20]:

$$\mu_s' = a\lambda^b \tag{6}$$

where a and b are parameters determined by the fitting.

sO_2 can be extracted from R_{SF} by curve fitting. In the phantom test, R_0 was measured before blood was added. In the *in-vivo* test, we assumed R_0 to be linear with wavelength, since the wavelength range is only 200 nm wide.

2.4. MC simulations for estimating sampled volume

To estimate the volume of tissue sampled by the single fiber system, MC simulations were performed using a modified version of MCML [21].

The tissue was modeled as a homogeneous slab with a refractive index of 1.36, and absorption and scattering specified by a total hemoglobin concentration of 50 μM and 2% intralipid, respectively, representative of brain tissue [2, 22, 23]. 160 million photons were injected into the layer at different oxygen saturations and wavelengths. For the photons that escape from the tissue within the numerical aperture and the diameter of the fiber, i.e. photons that can be collected by the system, the coordinates and strength of each absorption event are recorded. Finally, the strengths of all absorption events at each spatial coordinate were summed, convolved with a 200-μm-wide top-hat function to simulate incidence over the entire diameter of the fiber and plotted as a map of the absorption events of the collected signal. The map gives an indication of the location and the magnitude of the absorption, illustrating the spatial region that is sampled by the system.

2.5. System validation in an optical phantom

A phantom that mimics the optical properties of the brain [24] was used to test the performance of the single fiber system. The sO_2 of the phantom was decreased from ~100% to 0 by changing the gas composition in the environment.

OxyLite, a fluorescence-based system for measuring partial pressure of oxygen (pO_2) [6], was used as a reference system to estimate the accuracy of the single fiber system. The OxyLite system has a rated accuracy of ±10% in the range of 7-150 mmHg. To make the measurements of the single fiber system and the OxyLite comparable, the oxygen dissociation curve (ODC) for rat [25] was used to convert pO_2 to sO_2. The measured pO_2 values were first converted to pO_{2s}, the partial pressure of oxygen under the standard condition using Eq. (7) [25]:

$$pO_{2s} = pO_2 \times 10^{0.61(pH-7.4)} \tag{7}$$

where pH is the measured pH. Then, pO_{2s} is converted to sO_2 using Eq. (8) based on the ODC function [25]:

$$sO_2 = \frac{(pO_{2s})^n}{(pO_{2s})^n + (P_{50})^n} \times 100\% \tag{8}$$

Biomedical Optics EXPRESS

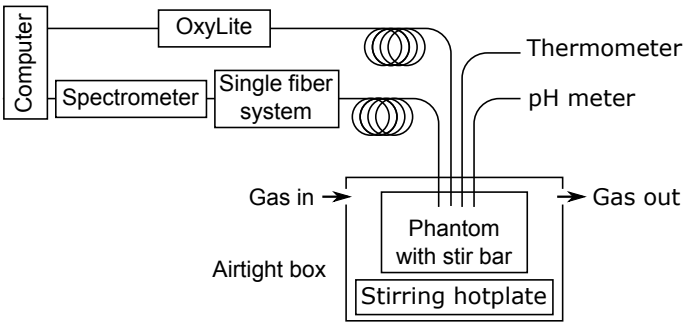

Fig. 3. A schematic drawing of the experimental setup for system validation in a phantom.

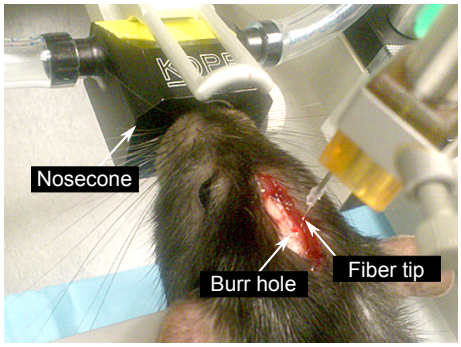

Fig. 4. Photograph of the experimental setup showing the fiber tip, burr hole for insertion and nosecone for oxygen control. Second burr hole for Oxylite probe insertion not shown.

where P_{50} is the half-saturation pressure. In rats, P_{50} is 36 mmHg and n is 2.6. Since the rat ODC used is valid only at 37°C and a pCO_2 of 40 mmHg, these two parameters were maintained at the respective values.

The phantom was composed of 800 μL of rat blood, 5 mL of 20% intralipid and 95 mL of PBS. The scattering and absorption effects were caused by 1% intralipid in PBS and rat blood, respectively.

Figure 3 shows the schematic drawing of the phantom experiment setup. The phantom was put in an airtight box. When the experiment started, the phantom was first oxygenated in 60% nitrogen, 34% oxygen and 6% carbon dioxide for 15 minutes. With the atmospheric pressure at our location being 670 mmHg, the percentages correspond to pN_2=402 mmHg, pO_2=227.8 mmHg and pCO_2=40.2 mmHg. Then, the phantom was kept in 94% nitrogen and 6% carbon dioxide (pN_2=629.8 mmHg, pO_2=0 and pCO_2=40.2 mmHg) for deoxygenation and the recordings started. Temperature was monitored by a thermometer and kept at 37±0.5°C by a hotplate stirrer. The pH of the phantom was measured every 3 minutes by the pH meter (FE20, Mettler Toledo, USA) with a precision of ±0.01 units.

2.6. *In-vivo measurements*

To test the system's ability to monitor sO_2 *in-vivo*, the fiber was implanted in the cortex in three C57 mice. The percentage of oxygen in the air that the animals breathed in was controlled and OxyLite was used as a reference system.

Figure 4 shows the experimental setup. The mice were anaesthetized by isoflurane inhalation (4% for induction and 1.5-2% for maintenance, 70% nitrogen and 30% oxygen). After a skin

Biomedical Optics EXPRESS

incision, two 1-mm-diameter holes were made in the skull using a dental drill above the cerebral cortex (coordinates: 0.7 mm anterior and ±1.5 mm lateral to bregma). Through one hole, tissue sO_2 was measured using the single fiber system at the depth of ~1 mm. Through the other hole, tissue pO_2 was measured using the OxyLite probe at about the same depth at 1 Hz. The experiment started 30 minutes after both probes were in the brain. The experiment started with animals breathing 30% oxygen, and then the percentage was changed to 20%, 15%, 10%, 8%, 0, 30% and 8%. Mice were sacrificed after experiments finished. All experiments were conducted in accordance with Canadian Council for Animal Care guidelines, and were approved by the Institutional Animal Care and Use Committee of the University of Calgary.

We expect that the sO_2 measured by the single fiber system and the pO_2 measured by OxyLite to show similar trends, because the tissue oxygen level resulting from controlling the air breathed in should be global. However, the calculated sO_2 and the reference pO_2 are not direct comparable for the following reasons. Firstly, a precise, local measurement of pH, temperature, and pCO_2 could not be done *in-vivo*. Also, unlike the phantom experiment where the sO_2 in the phantom was homogeneous, there may be differences in local brain activity causing inhomogeneous sO_2 distribution in the brain, with the single fiber system and the OxyLite measuring at two different locations. Thus, we did not calculate sO_2 from the measured pO_2.

3. Results and discussions

3.1. Sampled volume

Figure 5 shows the normalized maps of absorption events that contribute to the collected signal from the MC simulations on a linear scale, cut off at 10% of the maximum. For each figure, red represents the highest cumulative absorption among collected photons while blue presents the lowest. The simulations were performed at three different wavelengths in the spectral range that we use: 500, 600 and 700 nm, and at 0 and 100% sO_2. The interrogation volumes were estimated as cylinders and ranged from 0.02-0.03 mm^3.

While the actual volume is determined by the scattering and absorption properties of the sample and is wavelength-dependent, our simulations are an attempt to gauge the order of magnitude of the sampled volume. MC simulations for single fiber systems have been used to estimate path length and sampling depth [19]. To the best of our knowledge, an estimation of the spatial localization of the tissue being sampled has not been done before.

3.2. Phantom measurements

Figure 6(A) shows the calculated sO_2 vs. time. The reflectance spectra collected in the phantom before the blood was added was used as a measure of scattering in the phantom, R_0. The spectra were measured with an integration time of 0.7 s, and were averaged over 3 consecutive measurements to calculate sO_2. The calculated sO_2 values decrease monotonically with time, which matches the trends from the reference system. Due to the uncertainty in the pH and pO_2 measurements during the experiment, the reference value of sO_2 calculated from the pO_2 measured by the OxyLite was calculated with a higher and lower bound, indicated by the gray area in Fig. 6.

Figure 6(B) shows the calculated sO_2 along with the higher and lower bounds given by the pO_2 measurements in a phantom experiment. Compared with the reference, root mean squared error (RMSE) was 4.21%, and 63.10% of the measured sO_2 were within the bounds.

This error may be caused by the inaccuracy of the empirical fitting model or the absorption coefficients of hemoglobin. As previously reported by Amelink [26], using absorption coefficients of human hemoglobin from different sources, a maximum deviation of 9.5% in the sO_2 was observed in their system. Our experiments used rats and mice, whose absorption coefficients are quite distinct from human. To the best of our knowledge, the rat hemoglobin absorption

Biomedical Optics EXPRESS

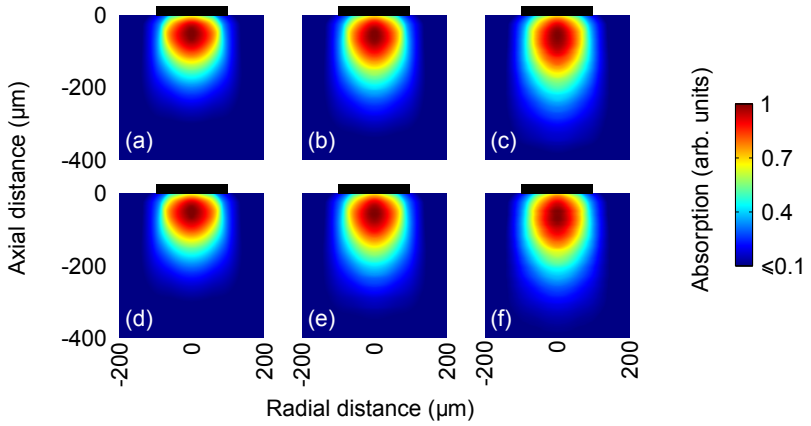

Fig. 5. Maps showing absorption events that contribute to the collected signal estimated using MC simulations. All simulations assume scattering from 2% intralipid and absorption from 50 μM hemolgobin. (a)-(c) 0 oxygen saturation at 500, 600 and 700 nm, respectively. (d)-(f) 100% oxygen saturation at 500, 600 and 700 nm, respectively. Black bar indicates fiber. Sampled volumes are 0.02-0.03 mm^3.

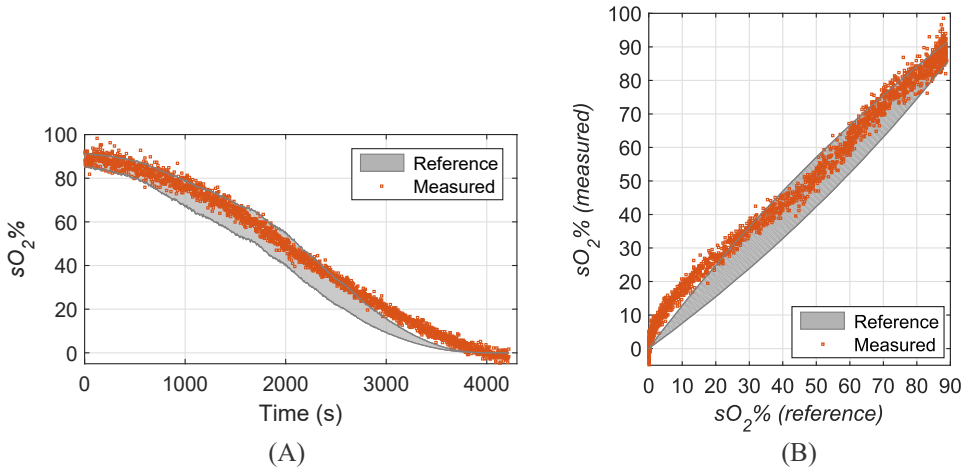

Fig. 6. The calculated sO_2 using the single fiber system in the phantom. Gray area shows the bounds given by the OxyLite system. (A) Calculated sO_2 as a time sequence. (B) Calculated sO_2 against the reference system.

coefficients we used are the only ones reported in the visible wavelengths [27]. Regardless, as found by Amelink, inaccuracies in the absorption coefficients could explain some of our errors.

3.3. *In-vivo measurements*

The spectra were measured with an integration time of 0.45 s, and were averaged over 2 consecutive measurements to calculate sO_2. Since the rate of hemodynamic changes is on the magnitude of seconds [28], the achieved temporal resolution is enough to monitor sO_2. The temporal resolution can be further improved by using a higher-power LED as the light source.

Figure 7 shows two measured reflectance spectra and the fitted spectra using Eq. (3), when the measured sO_2 were 56% and 0, and the molar absorption spectra of the corresponding HbO and Hb mixtures [27]. In both cases, the shape features of the measured reflectance spectra match

Biomedical Optics EXPRESS

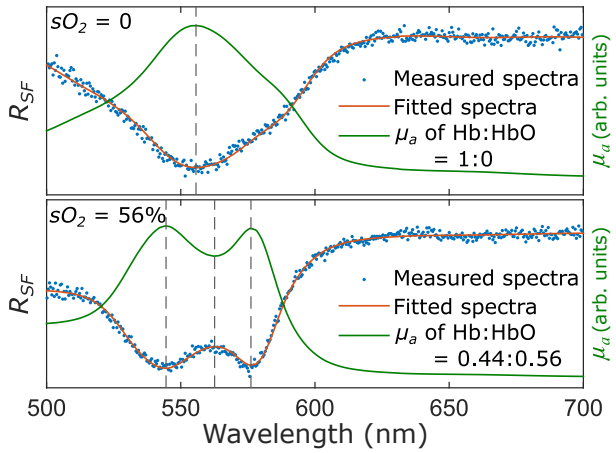

Fig. 7. R_{SF} and the fitted spectra when the measured sO_2 were 0 and 56%, and the molar absorption spectra of hemoglobin with Hb:HbO ratio of 1:0 and 0.44:0.56, corresponding to the sO_2 values. Peaks (valleys) in absorption agree well with lows (highs) in reflection.

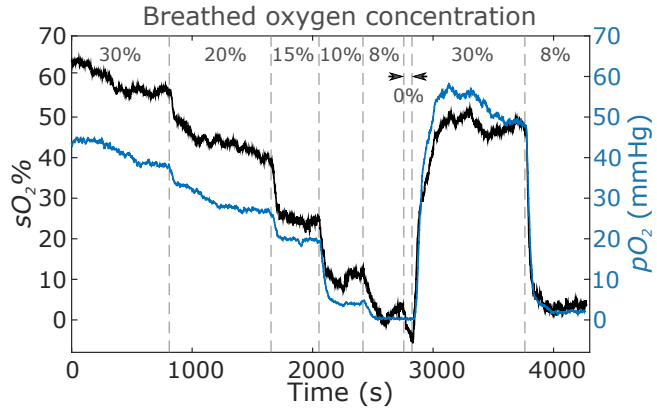

Fig. 8. The calculated sO_2 (black) and pO_2 measured by OxyLite (blue) vs. time *in-vivo* in one mouse. Dashed lines show the time of oxygen changes.

those of the molar absorption spectra of appropriate Hb:HbO mixtures, 1:0 and 0.44:0.56, for sO_2 of 56% and 0, respectively. The spectra can be fitted into the model with reasonable accuracy, which supports the linear assumption of R_0 and the correction method in Eq. (2).

Figure 8 shows the calculated sO_2 by the single fiber system and the pO_2 measured by OxyLite vs. time. The dashed lines show the time of oxygen changes. The calculated sO_2 is smoothed by a 5-sample sliding window. Changes of sO_2 can be observed right after the change of inhaled oxygen percentage. The measured sO_2 and pO_2 show similar trends as expected.

When the oxygen percentage in the inhaled air was lower than 8%, the system returned negative sO_2 values. One reason for this might be that the linear assumption ignores spectral features in R_0, the reflectance assumes no absorption. Another source of error is inaccurate hemoglobin absorption coefficients. In order to compensate for those using the spectra of HbO and Hb, the fitting process could return negative values. Another possibility is that the fitting process only considers HbO and Hb as chromophores. Under extreme conditions, e.g. when the inhaled oxygen percentage drops to 0, there may be other chormophores generated in response to anoxia. Negative sO_2 values are not realistic and from the point of view of an absolute

Biomedical Optics EXPRESS

quantification of sO_2, those readings should be bounded to 0. However, as seen in Fig. 8, if we do not constrain the fitting, the system is capable of resolving small relative changes in sO_2 as seen in going from 8% to 0% inhaled oxygen. It is worth noting that the Oxylite was not able to discriminate those conditions.

Though the implant of a small diameter fiber is minimally invasive, it is worth mentioning that the physical placement of a fiber into the brain may cause bleeding and trauma right after the implantation, and introduce artifacts to the local hemodynamics. In this acute experiment, we waited 30 minutes after the fiber was implanted before recording data. Ideally, chronic measurements should start after the tissue and blood vessels around the fiber tip have healed, a period that is unclear but may range to several days [7].

4. Summary

In this study, we presented a novel single fiber system for functional monitoring of tissue sO_2 from deep brain structures. Compared with previously reported reflectance systems, where halogen lamps with rated power of tens to hundreds watts are typically used as light sources, the reported system is very power efficient with a warm white LED driven by 60 mW electrical power as the light source. The system avoids the use of bifurcated fibers, giving it the potential for future miniaturization for measurements in freely-moving animals. The simplified calibration methods make it convenient to be used.

We tested the performance of the single fiber system in an optical phantom. Compared to the reference system, the single fiber system showed reasonable temporal resolution, accuracy and sensitivity. We experimentally demonstrated, for the first time, continuous highly-localized measurement of sO_2 in the brain using the single fiber system. Sources of error may come from the linear approximation of R_0, using glycerin-water solution as an estimation of Fresnel reflection and considering hemoglobin as the sole chromophore.

To summarize, this single fiber system allows tissue sO_2 measurement to be done in a very localized volume over time at any depth in the brain. It provides a new method for optically interrogating deep brain hemodynamic activity.

Funding

This research was supported by Natural Sciences and Engineering Research Council (NSERC) RGPIN/418976, RGPIN-2015-06517 and CMC Microsystems emSYSCAN.